# Recognizing fracture pattern signatures contributed by seismic loadings

Shiqing Xu[1*]

[1]Department of Earth and Space Sciences, Southern University of Science and Technology, Shenzhen 518055, China

[*]Corresponding author: xusq3@sustech.edu.cn

**This paper is a non-peer reviewed preprint submitted to EarthArXiv. It has been submitted to *Interpretation* and is currently under peer review.**

## Abstract

The impacts of seismic loadings to fault zone rocks are still not well understood. While field and experimental studies have suggested several markers, such as pseudotachylytes and pulverized rocks, for indicating seismic loadings, the corresponding markers of other types or at larger scales are still lacking. Here by summarizing results of dynamic ruptures with off-fault damage, we recognize several additional fracture features that may be used to reflect the involvement of seismic loadings. For strike-slip faults stressed at moderate to high angles, synthetic R shear is more favored during rupture propagation, but pronounced antithetic R’ shear can be generated around the termination end of the rupture. In addition, suitably oriented weak structures off the main fault can further facilitate the activation of R’ shear. For low-angle thrust faults such as subduction zones, splay faults in the form of forethrusts and backthrusts can still be generated above the coseismic rupture zone. These faults show an increased spatial extent towards the updip direction, effectively defining an outer wedge susceptible to pervasive compressional failure over its entire depth range. Moreover, a deeply nucleated megathrust rupture that eventually reaches the trench can sequentially load the frontal wedge in compression and then in extension, with a potential to leave a mixture of triggered reverse and normal faults at the final stage. Because the above results are also supported by many observations, they raise a caution that existing fault models ignoring dynamic effects should be used with care, and that seismic loadings must be considered more seriously by future fault zone studies.


## Introduction

Natural fault zones are complex, often displaying a hierarchical structure of fractures, various types of geometrical irregularities, competent and incompetent material heterogeneities, and transformation of mineral phases (Green II et al., 2015; Collettini et al., 2019; Scholz, 2019). These complexities have two sides. On one hand, they complicate the study of fault zones by requiring additional knowledge from other fields (mechanics, physics, chemistry, etc.). On the other hand, they provide geoscientists with observable features that can be used to understand the formation and evolution of fault zones. Motivated by the positive side of fault zone complexities, many observational and theoretical works have attempted to classify fault zone categories and to build fault zone models. For reference, there are already literature reviews on fault zones in general (Caine et al., 1996; Ben-Zion and Sammis, 2003; Wibberley et al., 2008; Faulkner et al., 2010), on rock frictional properties (Marone, 1998; Scholz, 1998; Tullis, 2007; Di Toro et al., 2011), on the relation between faults, fractures, and stress (Pollard and Segall, 1987; Blenkinsop, 2008; Anders et al., 2014), and on the aseismic and/or seismic aspects of fault zones (Spray, 2010; Niemeijer et al., 2012; Rowe and Griffith, 2015; Bürgmann, 2018). Among these topics, to understand the contributions from earthquakes to fault zone properties is of particular interest, because seismic loadings are transient but extreme, the related predictions can be frequently tested, and the results have a direct impact to the human society.

To date, there is still much debate on the reliable markers for seismic loadings, but it is generally accepted that pseudotachylytes and pulverized rocks are two clear records of seismic loadings preserved in fault zone rocks (Rowe and Griffith, 2015). Their qualifications as seismic markers are supported by experimental constraints that require fast slip rate to produce frictional melting, and high strain rate to produce pervasive fracturing. Some studies further suggest that pulverized rocks and pseudotachylytes could be sequentially generated during a single earthquake rupture (Spray, 1995; Petley-Ragan et al., 2019). Despite the important value, to unambiguously observe pseudotachylytes and pulverized rocks is not easy, which can only be made in active or exhumed ancient fault zones that have not been significantly altered since the last episode of seismic activities (Kirkpatrick and Rowe, 2013). Moreover, the analyses of pseudotachylytes and pulverized rocks are often done at the outcrop or microscopic scale, making it difficult to capture the overall picture of earthquake characteristics at larger scales. These limitations with pseudotachylytes and pulverized rocks then lead to a question of whether other alternative features can be used to complement the identification of seismic loadings.

In this paper, we aim to address the aforementioned question by illuminating the relation between several fracture pattern signatures and seismic (or dynamic) loadings. Hereafter, the two terms seismic loadings and dynamic loadings are used interchangeably, with a focus on earthquake-generated fractures. Specifically, we compare fault models under both static and dynamic loadings, trying to understand the differences in the predicted fracture patterns off the main fault, especially at large scales. We discuss simulation results of earthquake ruptures in association with supporting examples from observations, utilizing signals accessible to both geological and seismological observations. With these efforts, we provide a refined understanding of fault zone evolution contributed by seismic loadings.

## Reference fault models and methods

To facilitate the comparison, we consider strike-slip faults and thrust faults separately. There are several reasons for such consideration: (1) the principal stress orientation relative to the main fault differs between the two (Scholz, 2019); (2) the location of off-fault damage with respect to the main fault also differs (Templeton and Rice, 2008); (3) there can be a continuous renewal of materials (e.g. sediments) and geometrical irregularities (e.g. subducting ridges and seamounts) for a thrust fault, whereas such renewal is generally lacking for a strike-slip fault (Wang, 2010); (4) the way of interacting with the free surface differs between the two; and (5) additional factors such as gravity and plate bending can play a role for a thrust fault.

Fig. 1 schematically shows several types of secondary fracture that can be found around a strike-slip fault (Fig. 1a, map view) and a subduction-type thrust fault (Fig. 1b, side view). Of particular interest to this study are the mode-II synthetic and antithetic shear fractures. Here, the use of synthetic (or antithetic) refers to the sense of shear that is consistent with (or opposite to) that along the main fault. In the case of Fig. 1b, the plate interface is taken as the main fault, while the associated synthetic and antithetic fractures are also known as forethrusts and backthrusts, respectively. It is worth mentioning that the various features illustrated in Fig. 1 only serve as a reference, but do not necessarily hold valid everywhere. Especially, one should note that wall damage zone and linking damage zone (Kim et al., 2004) are not included in Fig. 1a, and that there are many different types of subduction zone (Noda, 2016).

The methods for performing numerical simulations have already been described in detail elsewhere (Xu and Ben-Zion, 2013; Xu et al., 2015; Xu et al., 2016), so below we briefly recap some key components of the numerical model. We use the spectral element code SEM2DPACK (https://github.com/jpampuero/sem2dpack) to simulate 2D in-plane dynamic ruptures under a uniform or a depth-dependent initial stress field. In the numerical model a slip-weakening friction law governs the fault behavior, while a Mohr-Coulomb-type plasticity describes the response of off-fault medium to stress. The occurrence of plasticity is supposed to simulate the generation of off-fault damage. There is no post-yield weakening or hardening in the adopted plasticity. A characteristic timescale is used to tune the expressed form of plasticity, either as discrete shear bands when the timescale is small or as smoothly distributed plastic strain when the timescale is large. The parameter values for initial stress, fault friction, and off-fault plasticity are selected such that only sub-Rayleigh ruptures are generated. We keep the model as simple as possible to focus on the most fundamental features. Quadrilateral meshes are used to discretize the simulation domain. The effects of mesh size and mesh orientation have been rigorously tested, such that the key results to be discussed below are not significantly influenced by the employed mesh configuration (Xu and Ben-Zion, 2013).

**Strike-slip faults: Riedel shear structures**

We start with the Riedel shear structures that have been well documented by many field observations and analogy experiments (Tchalenko, 1970; Wilcox et al., 1973). While such structures can be observed in a variety of faulting regimes (Arboleya and Engelder, 1995; Davis et al., 1999), we decide to focus on the strike-slip regime. In the most standard case, elements generated in a Riedel shear system include tensile fracture T, synthetic shear fractures R, P, and Y, and antithetic shear fracture R' (Fig. 2a). Typically these elements are distributed on both sides of the final principal slip zone and can display en échelon patterns along the general strike direction. Hierarchical structures accompanied by secondary and higher-order branches can also be involved, which generally show increased structural complexity toward the direction with increased shear displacement (Ahlgren, 2001). Field and experimental studies suggest that the development of shear fractures cannot proceed by their own, but often involve the generation, interaction, and coalescence of other types of fractures (Segall and Pollard, 1983; Petit and Barquins, 1988). Combining with other seismological and geodetic observations, Ben-Zion and Sammis (2003) conclude that natural faults in their lifetime experience a long-term evolutionary process from distributed deformation (e.g. P, R, and R' shears) to localized deformation (principal slip zone), during which a gradual smoothing of the fault surface may also occur (Brodsky et al., 2011).

The corresponding Riedel shear structures generated during earthquakes show several features that are notably different from their quasi-static counterparts mentioned above. First, the overall strain partitioning during earthquakes includes a component of delocalization (Ando and Yamashita, 2007), manifested by a large set of fresh fractures activated off the main fault (Fig. 2b). A related feature revealed by some laboratory observations is the trend of fault surface roughening, rather than smoothing, during high-speed rupture propagation (Xu et al., 2018; Yamashita et al., 2018). Second, the newly generated fractures are primarily distributed on one side of the fault, which is the extensional side for a fault stressed at moderate to high angles. Third, the pattern of off-fault fractures shows increased structural complexity, such as the development of higher-order branches (e.g. zoom-in window II in Fig. 2b), towards the rupture propagation direction. For a crack-like rupture this is the direction with decreased shear displacement. Fourth, the in situ orientations of R and R' shears show a clockwise rotation relative to the ones expected from the background principal stress $\sigma_{\max}$. In particular, R' shear can be orientated in the backward direction (i.e. with an obtuse angle relative to the rupture propagation direction). Overall, the above features can be explained by the following effects when rupture speed becomes high and/or when rupture propagation distance becomes long: the optimal failure plane around the rupture front shifts off the main fault (Poliakov et al., 2002), there is enough energy for activating multiple fractures (Fineberg and Marder, 1999), the off-fault stress amplitude increases (Freund, 1998), and the in situ principal stress axis on the extensional side rotates towards the fault-normal direction (Rice, 1980; Ngo et al., 2012).

Despite the above differences, the Riedel shear structures generated during rupture propagation can share some phenomenological features with their quasi-static counterparts, such as a possible prevalence of R shear over R' shear (Fig. 2b, beyond section I). However, the underlying mechanisms are quite different. For the quasi-static case, the dominance of R shear is attributed to the fact that R shear is less rotated than R' shear. As a result, R shear can sustain a favorable orientation to accommodate additional shear displacement (Wilcox et al., 1973). For the dynamic case, R shear is more favored for its growth direction following that of rupture propagation. Accordingly, R shear can benefit from the dynamic stress field around the propagating rupture front over a longer time duration than R' shear (Xu and Ben-Zion, 2013). The changing rupture front configuration is a feature unique to seismic loadings. It introduces a directivity effect that tends to favor low-angle branching over high-angle branching, or forward branching over backward branching during rupture propagation.

It is important to emphasize that an earthquake rupture cannot propagate forever, but will terminate either because it runs out of the energy or because it encounters some sort of barrier (Bayart et al., 2018; Ke et al., 2018). Upon an abrupt rupture termination, the rupture front no longer changes its position significantly over time, such that the directivity effect mentioned above will cease to operate. A byproduct of abrupt rupture termination is the enhancement of stress amplitude around the rupture front (which scales with the stress intensity factor), due to a nearly instantaneous reduction of rupture speed (Freund, 1998). As a result, one may expect both forward and backward shear branches can be equally favored. Such expectation is indeed confirmed by the simulation result, which shows well-developed R and R' shears around the barrier where a propagating rupture abruptly terminates (Fig. 2c). Beyond the coexistence of R and R' shears, it is interesting to note that these newly formed shear branches together with the original main fault form a triple junction pattern (see inset in Fig. 2c) similar to the one introduced by King and Nábělek (1985). Moreover, the result that the angle opposite to the antithetic R' shear is larger than $180^{\circ}$ is entirely consistent with the model prediction by Andrews (1989).

## Influence of preexisting plane of weakness

So far results are discussed by assuming no preexisting structures off the main fault, but such assumption could be oversimplified. In nature, major faults are sometimes surrounded by structures (e.g. low velocity zones, fracture zones, spreading ridges, magnetic anomalies, and rotated R' fractures) inherited from earlier or other tectonic activities, and fault systems consisting of multiple sub-parallel or conjugate segments do exist (Nicholson et al., 1986; Talwani, 2014; Ross et al., 2017; Lay, 2018; Das, 2019). It is therefore important to investigate how preexisting structures may influence the pattern of strain partitioning during earthquakes. Specifically, we are interested in how a preexisting weak plane, when inserted at a suitable place (e.g. where off-fault damage can be expected), can change the damage pattern compared to the situation without the weak plane.

We consider two cases (Fig. 3) similar to the ones in Figs. 2b and c, but now with a preexisting branch fault located on the extensional side of the main fault. Note that for the current cases the sense of shear is set as left lateral for the main fault, meaning that the shear directions along R and R' need to be updated as well. The inclination angle of the branch fault is fixed at $100^{\circ}$, aiming to closely match the anticipated direction of R' shear (Fig. 3). To facilitate the comparison between distributed and localized deformation, now a relatively large timescale is assumed for the bulk plasticity, ensuring a continuously smooth distribution of the generated plastic strain. Similar to the treatment for the main fault, a slip-weakening friction law is adopted to control the slip behavior along the branch fault.

Let's first focus on the results on the right half of the domain. When there is no barrier (here barrier means an increase of fault strength) to interrupt the rightward propagation of the rupture along the main fault, the branch fault can still be activated but with a limited amount of antithetic (right-lateral) slip no more than 0.83 m (Fig. 3a). Moreover, the triggered rupture along the branch fault finally dies out, leaving a confined rupture zone extent less than 10 km. As a result, the feedback from the branch fault to the main fault is also limited. For example, the perturbation to the plastic strain field associated with the main fault mainly occurs for portions near the fault junction. Far from the junction, the plastic strain field returns to a self-similar triangular pattern, as if the branch fault were never activated. The situation is quite different when there is a barrier to abruptly terminate the rightward rupture along the main fault. Now the branch fault accommodates a triggered rupture that can sustain its outward propagation away from the junction, with a rupture zone extent at least as large as 15 km (Fig. 3b). Associated with this sustained rupture is a narrow belt region of plastic strain distributed on the extensional side of the branch fault.

To better see the influence of the inserted branch fault, we compare the results to the left with those to the right. In the left direction, plasticity is the sole form of inelastic strain distributed off the main fault. Near the left barrier, a conjugate set of plastic shear bands is generated, with a maximum off-fault thickness slightly less than 5 km. In the right direction and particularly around the branch fault, inelastic strain takes place in a very localized form, presumably dominated by the triggered slip along the branch fault. It appears that the preexisting branch fault has collapsed most (if not all) of the anticipated plastic strain in its vicinity, by converting it to slip. Moreover, the slip-weakening mechanism along the branch fault allows slip to extend further, more than 5 km away from the main fault. From these observations, we see that preexisting plane of weakness not only can lead to strain localization but also can promote instability via some weakening mechanisms.

The above results (Fig. 3) along with those presented in the previous section (Figs. 2b and c) lead to a testable prediction, which states that abrupt rupture termination along strike-slip faults can produce orthogonally or backward oriented antithetic branching on the extensional side of the main fault. The antithetic branching may manifest itself as (1) coseismically triggered secondary rupture, (2) triggered secondary rupture with apparent time delays, (3) triggered aseismic slip, or (4) aftershock clusters, depending on nearby preexisting structures, regional stress, fault zone properties, and other conditions. Indeed, many observational works have confirmed the predicted feature of antithetic branching. Examples of category (1) include the Wharton Basin earthquake sequences in 2000 (Robinson et al., 2001) and in 2012 (Meng et al., 2012), the earthquake sequence observed in the laboratory (Rousseau and Rosakis, 2003), the 2014 $M_w$ 6.9 Yutian earthquake (Li et al., 2016), and the $M_w$ 6.4 event during the 2019 Ridgecrest earthquake sequence (Ross et al., 2019). Examples of category (2) include the 1987 Superstition Hills earthquake sequence (Hudnut et al., 1989), and the 2005 earthquake sequence in western Turkey (Aktar et al., 2007). One example of category (3) is the triggered creep along the Garlock fault following the 2019 Ridgecrest earthquake sequence (Barnhart et al., 2019). Examples of category (4) include aftershocks to the west of the 1989 Macquarie Ridge earthquake rupture zone (Das, 1992), aftershocks to the northeast of the 1992 Landers earthquake rupture zone (Hauksson et al., 1993), aftershocks to the south of the 1998 $M_w$ 8.0 Antarctic Plate earthquake rupture zone (Henry et al., 2000), aftershocks to the southwest of the 2011 $M_w$ 6.4 Skyros earthquake (Karakostas et al., 2003), and aftershocks following the 2003 $M_w$ 5.0 Big Bear earthquake (Chi and Hauksson, 2006). More examples of antithetic branching or conjugate earthquake faulting can be found in Das and Henry (2003), Fukuyama (2015), and Das (2019).

**Thrust faults: the Coulomb wedge model**

As mentioned earlier, subduction-type thrust fault systems often display several features that cannot be simply accounted for by the generic fault model for strike-slip faults. So here we present a separate comparison among different models for subduction zones, focusing on the deformation in the frontal wedge of the overriding plate.

A classical model dealing with the deformation of the frontal wedge is the Coulomb wedge model (Davis et al., 1983; Dahlen, 1984; Dahlen et al., 1984). This model considers the static stress equilibrium between tectonic loading, gravity, and basal friction, for situations where wedge geometry and pore fluid pressure are taken into account. It states that eventually the entire wedge will be on the verge of Coulomb failure everywhere and therefore at or near a critical state. Upon reaching the critical state, the slip line theory (Hill, 1950) can be applied to depict the potential failure planes within the wedge and along its base, which depending on the detailed conditions could correspond to either thrust faulting or normal faulting. For illustration, a wedge at compressionally critical state is shown in Fig. 4a. The model itself does not directly consider any time-dependent process, leaving the geometry and the internal structure of the wedge largely stationary over time. In reality, sediments must be slowly added to (or removed from) the wedge, such that the actual process for retaining a critical state should be better understood as quasi static. Because the mechanical and geometrical properties of the wedge are linked, the model can be applied to infer the basal friction or the internal friction from the wedge slope and orientations of the internal faulting.

One problem with the classical Coulomb wedge model is that the assumption of static stress equilibrium (i.e. lack of time-dependent modulation or inertial effects) may not always hold. This is particularly the case for margins known to host great ($M_w \geq 8.0$) earthquakes, such as Chile, Japan Trench, and Sumatra (Bilek and Lay, 2018). Detailed observation made on several accretionary wedges reveals a spatial variation of deformation styles: the most seaward part (outer wedge) is generally more deformed than its landward neighbor (inner wedge). Additional lines of evidence also suggest an updip limit for the coseismic rupture zone in subduction zones (Byrne et al., 1988; Hyndman et al., 1997). These have led Wang and Hu (2006) to propose a dynamic version of the Coulomb wedge model, by taking into account time-dependent modulation throughout earthquake cycles. In their model, the basal friction condition is characterized by velocity weakening for the inner wedge and velocity strengthening for the outer wedge (Fig. 4b).

During the interseismic stage, both the inner and outer wedges are likely to stay in a stable regime (Fig. 4b, left panel), due to the stress drop from the previous earthquake in the seismogenic zone and the "protection" (or "shadowing") effect of the locked seismogenic zone on the updip zone (Wang and Hu, 2006; Almeida et al., 2018). During the coseismic and earlier postseismic stages, basal shear stress along the seismogenic zone drops again, further removing the inner wedge away from a compressionally critical state; at the same time, seismic slip within the seismogenic zone transfers stress to the updip zone, which together with the underlying velocity-strengthening friction can push the outer wedge into a compressionally critical state (Fig. 4b, right panel). Therefore, in the light of this dynamic Coulomb wedge model, it is mainly the outer wedge that can episodically enter a compressionally critical state.

Furthermore, recent studies also suggest that some megathrust earthquakes can propagate into the updip zone or even reach the trench (Hubbard et al., 2015), which then raises the question of whether compressional structures such as splay faults can still be generated right above the coseismic rupture zone. A series of papers on this topic suggest a positive answer and reveal the underlying reason (Ma, 2012; Ma and Hirakawa, 2013; Xu and Ben-Zion, 2013; Xu et al., 2015). During the coseismic stage, stress drop does not occur simultaneously over the entire seismogenic zone; rather, it is directed by a propagating rupture front, first from the hypocenter and then spreading out with a finite speed. The rupture front defines a dynamic basal boundary that separates portions undergoing transient strengthening (still locked) from those experiencing frictional weakening (already slipped) (Fig. 4c, left panel). It is the universal transient strengthening effect ahead of the rupture front (due to stress transfer from the behind slipping zone) that is responsible for activating splay faults in the overriding plate (Xu et al., 2015), with no need to invoke an initial strengthening mechanism in the adopted friction law. Such interpretation is indeed supported by the simulation result that compressional failure modeled as plastic shear bands can be generated above a coseismic rupture zone governed by slip-weakening friction (Fig. 4c, right panel), by the experimental result that permanent contraction can be accumulated above a seismogenic zone governed by velocity-weakening friction (Rosenau and Oncken, 2009), and by the natural observation that new compressional structures were generated in the frontal wedge during the 2011 trench-breaking Tohoku earthquake (Kodaira et al., 2012). It is worth mentioning that in Fig. 4c the compressional structures show an increased vertical extent towards the updip direction, with a potential to saturate the local depth range of the wedge near the trench. This is opposite to the prediction of the classical Coulomb wedge model (Fig. 4a), but would provide an alternative explanation for the inner-outer wedge contrast invoked by Wang and Hu (2006).

**Sequential wedge deformation during a single earthquake**

One enigmatic observation of fracture patterns is the coeval development of both reverse and normal faults, as documented by the deformation in the Mauna Loa-Kilauea rift system in Hawaii (Yin and Kelty, 2000), by the aftershock focal mechanisms following the 1989 Loma Prieta earthquake (Beroza and Zoback, 1993) and the 2011 Tohoku earthquake (Hasegawa et al., 2012), by the seismic survey over the Japan Trench (Boston et al., 2017), and by the fracture network around a subducting seamount (Dominguez et al., 2000) or a thrust ramp (Bonini et al., 2000). Two general mechanisms have been proposed. One invokes spatial heterogeneity such that the in situ stress field, fault strength, or fault orientation varies from place to place. The other suggests a time-varying process such that the same region may sequentially experience multiple episodes of loading with changing polarities. Below we focus on the second mechanism and try to understand the origin of some upper-plate structures observed in the Japan Trench.

We consider a megathrust rupture scenario that closely mimics the 2011 Tohoku earthquake (Ide et al., 2011). The rupture is nucleated at depth, deeper than the base of the frontal wedge. At the earlier stage before the rupture reaches the trench, the evolving slip profile of the megathrust rupture displays a semi-elliptical shape, still having its peak slip at depth (Figs. 5a and c). This imposes a transient compression to the updip frontal wedge, whose base is still locked but experiencing a transient increase of shear stress. Detailed Coulomb stress calculations show that a hypothetic branch fault, dipping either seaward or landward in the frontal wedge, can accommodate a triggered reverse sense of slip at this earlier stage (Xu et al., 2016).

However, the situation dramatically changes after the megathrust rupture reaches the trench. Because of the extremely low (nearly zero) stiffness beyond the trench axis, the stress concentration around the updip rupture front has to be relaxed upon reaching the trench (Dmowska and Kostrov, 1973). This can cause suddenly amplified slip near the trench and “reflected” phases (e.g. fault-interface Rayleigh wave) preserving the original slip direction towards the downdip direction (McLaskey et al., 2015; Gabuchian et al., 2017; Xu et al., 2019). One remarkable feature at this stage is that slip can accumulate freely without additional stress drop (Xu et al., 2019). As a result, shear stress beneath the frontal wedge is released, the overall slip profile changes to a quarter-elliptical shape with its peak at or near the trench, and the average level of slip becomes twice (or more) of that at the earlier stage (Geist and Dmowska, 1999). Correspondingly, the stress state within the frontal wedge changes from compression to extension, which can reactivate a hypothetic branch fault with a normal sense of slip (Figs. 5b and d).

Now we prove the possibility that the frontal wedge can sequentially experience compression followed by extension during a single megathrust earthquake. After being shaped by many Tohoku-type megathrust earthquakes, the frontal wedge in its present form may preserve a record of both reverse and normal faults, or faults having opposite senses of slip at different depth sections (Xu et al., 2015). This provides a possible alternative explanation for the observed upper-plate faulting structures at both microscopic and macroscopic scales in the Japan Trench (Tsuji et al., 2013; Keren and Kirkpatrick, 2016; Boston et al., 2017). It should be emphasized that the key ingredients for the above mechanism are the existence of a free surface boundary (or boundary with a strong stiffness/impedance contrast) and the action-reaction dynamics operated near that boundary, without requiring a friction-related dynamic overshoot along the basal plane (Ide et al., 2011). In this regard, the above mechanism can also be applied (and indeed has been applied) to other phenomena even without the participation of basal friction, such as the generation of both low-angle and high-angle tensile cracks in rocks during an impact and spalling test (Cho et al., 2003).

## Discussion and conclusions

Based on results of dynamic rupture simulations, we have recognized several fracture pattern signatures in close association to seismic loadings. They include the pronounced antithetic fault branching upon rupture termination along a strike-slip fault, the coseismic activation of splay faults above a megathrust fault, and the sequential activation of reverse faults and normal faults in the frontal wedge during a trench-breaking megathrust earthquake. In addition, we have also found many observational examples, reported both in the laboratory and in natural fault zones, to support the related fracture patterns. The general consistency between simulations and observations suggests that the results are likely to be robust, which therefore can help improve the understanding of fault zone structures contributed by seismic loadings.

Unlike the previously proposed use of rock textures (e.g. for pseudotachylytes and pulverized rocks), fracture patterns can be analyzed by both direct geological mappings and indirect seismological observations. This greatly extends the availability of datasets, e.g. by including buried earthquakes and remote earthquakes, such that more observational examples can be used to test the related model predictions. It also facilitates a validation of model predictions across different disciplines. For example, results derived from seismic profiles can be combined with other information to help understand the origin of the imaged fracture patterns (Liao et al., 2019; Hananto et al., 2020). Another advantage of using fracture patterns can be attributed to their capability of reflecting large-scale earthquake dynamics, such as the triple junction pattern formed around an earthquake termination end (Fig. 2c) and the kilometer-scale earthquake triggering between two conjugate faults (Fig. 3).

One important aspect of seismic loadings is that their effects are transient, mainly during the stages of earthquake propagation and termination. In most cases, coseismically activated fractures will become "frozen" once the main rupture front has passed by (Fig. 4c, left panel). One exception is that the activated fractures (or triggered secondary ruptures along preexisting structures) can sustain their subsequent growth via some weakening mechanisms (Ando and Yamashita, 2007; Xu et al., 2015). In any case, the in situ stress field responsible for initiating fractures or sustaining their subsequent growth can be quite different from the regional background stress. Therefore, caution must be taken when using observed fracture properties, such as their orientations, to infer the regional background stress or fault zone rheology (Anderson, 1905; Sibson, 1985). For example, the occurrence of an earthquake sequence along two orthogonal faults does not necessarily mean a low fault friction is at play (Thatcher and Hill, 1991; Xu and Ben-Zion, 2013). Similarly, the appearance of internal structures in the frontal wedge does not necessarily imply the wedge always stays at a critical state, especially for the case in earthquake-prone subduction zones (Figs. 4b and c). Caution should also be taken when attempting to interpret mixed fracture modes or fracture orientations preserved in the field, because time-dependent overprinting can play an important role (Fig. 5).

Another important aspect of seismic loadings is that the associated strain rate can be extremely high, orders of magnitude higher than the tectonic strain rate (Spray, 2010).

High strain rate has been invoked to explain the generation of pulverized rocks characterized by pervasive tensile cracking (Rowe and Griffith, 2015). Likewise, high strain rate may also be responsible for the initiation of shear branching, given its intimate relation with energy rate (Freund, 1998). Perhaps we could unify pulverized rocks and some shear branching features presented in this study, and treat both of them as damage patterns indicative of high strain rate. Usually it is difficult to excite high strain rate broadly across a large intact domain. Nevertheless, the emergence of high strain rate can be facilitated by the existence of weak structures. When there is a suitably oriented branch fault near the main fault, a secondary rupture can be triggered along the branch fault, with an ability to extend high strain rate and hence severe damage further away from the main fault (Fig. 3). This has a direct implication for reconsidering the distributions of fracture density and seismic intensity around a master seismogenic fault (Okubo et al., 2019; Ma and Elbanna, 2019).

Finally we shall be aware of some issues that may affect the findings of this study. First, while we have successfully linked several fracture patterns with seismic loadings, the interpretations for those fracture patterns may still be non-unique. This issue will become more urgent for evaluating patterns preserved in ancient fault zones, when only field observations are available. Second, seismic waves can have an enormous impact to the damage patterns near the Earth's surface (Ma and Andrews, 2010) and can trigger events over a considerable distance (Brodsky and van der Elst, 2014). However, their effects have not been fully taken into account in this study. Third, off-fault damage patterns can be modified by other additional factors, including fault geometrical complexity (Dunham et al., 2011; Goebel et al., 2017), material heterogeneity (Bürgmann et al., 1994; Ben-Zion and Shi, 2005), and supershear ruptures (Bhat et al., 2007). Fourth, it remains unclear the respective contribution to the present-day fault zone structures from aseismic loadings, seismic loadings, various types of relaxation, and other processes (Wang et al., 2010; Perrin et al., 2016; Jamtveit et al., 2019; Preuss et al., 2019). Definitely, continued efforts are required to achieve a more complete understanding of fault zones. One promising direction is to study earthquake cycles in conjunction with multidisciplinary observations.

**Acknowledgments**

We thank Eiichi Fukuyama, Yehuda Ben-Zion, Jean-Paul Ampuero, and Vladimir Lyakhovsky for discussion and collaboration over the past years. We thank Guest Editor Zonghu Liao for the invitation. Brett Carpenter and an anonymous reviewer provide useful comments that help improve the quality of the manuscript. This work was partially supported by S. Xu's startup fund from Southern University of Science and Technology, China.

## References

Ahlgren, S. G., 2001, The nucleation and evolution of Riedel shear zones as deformation bands in porous sandstone: Journal of Structural Geology, **23**, no. 8, 1203–1214, doi: 10.1016/S0191-8141(00)00183-8.

Aktar, M., H. Karabulut, S. Özalaybey, and D. Childs, 2007, A conjugate strike-slip fault system within the extensional tectonics of Western Turkey: Geophysical Journal International, **171**, no. 3, 1363–1375, doi: 10.1111/j.1365-246X.2007.03598.x.

Almeida, R., E. O. Lindsey, K. Bradley, J. Hubbard, R. Mallick, and E. M. Hill, 2018, Can the updip limit of frictional locking on megathrusts be detected geodetically? Quantifying the effect of stress shadows on near-trench coupling: Geophysical Research Letters, **45**, no. 10, 4754–4763, doi: 10.1029/2018GL077785.

Anders, M. H., S. E. Laubach, and C. H. Scholz, 2014, Microfractures: A review: Journal of Structural Geology, **69**, 377–394, doi: 10.1016/j.jsg.2014.05.011.

Anderson, E. M., 1905, The dynamics of faulting: Transactions of the Edinburgh Geological Society, **8**, 387–402, doi: 10.1144/transed.8.3.387.

Ando, R., and T. Yamashita, 2007, Effects of mesoscopic-scale fault structure on dynamic earthquake ruptures: Dynamic formation of geometrical complexity of earthquake faults: Journal of Geophysical Research: Solid Earth, **112**, B09303, doi: 10.1029/2006JB004612.

Andrews, D. J., 1989, Mechanics of fault junctions: Journal of Geophysical Research: Solid Earth, **94**, B7, 9389–9397, doi: 10.1029/JB094iB07p09389.

Arboleya, M. L., and T. Engelder, 1995, Concentrated slip zones with subsidiary shears: their development on three scales in the Cerro Brass fault zone, Appalachian valley and ridge: Journal of Structural Geology, **17**, no. 4, 519–532, doi: 10.1016/0191-8141(94)00079-F.

Barnhart, W. D., G. P. Hayes, and R. D. Gold, 2019, The July 2019 Ridgecrest, California, earthquake sequence: Kinematics of slip and stressing in cross-fault ruptures: Geophysical Research Letters, **46**, no. 21, 11859–11867, doi: 10.1029/2019GL084741.

Bayart, E., I. Svetlizky, and J. Fineberg, 2018, Rupture dynamics of heterogeneous frictional interfaces: Journal of Geophysical Research: Solid Earth, **123**, no. 5, 3828–3848, doi: 10.1002/2018JB015509.

Ben-Zion, Y., and C. G. Sammis, 2003, Characterization of fault zones: Pure and Applied Geophysics, **160**, no. 3-4, 677–715, doi: 10.1007/PL00012554.

Ben-Zion, Y., and Z. Shi, 2005, Dynamic rupture on a material interface with spontaneous generation of plastic strain in the bulk: Earth and Planetary Science Letters, **236**, no. 1-2, 486–496, doi: 10.1016/j.epsl.2005.03.025.

Beroza, G. C., and M. D. Zoback, 1993, Mechanism diversity of the Loma Prieta aftershocks and the mechanics of mainshock-aftershock interaction: Science, **259**, no. 5092, 210–213, doi: 10.1126/science.259.5092.210.

Bhat, H. S., R. Dmowska, G. C. King, Y. Klinger, and J. R. Rice, 2007, Off-fault damage patterns due to supershear ruptures with application to the 2001 $M_w$ 8.1 Kokoxili (Kunlun) Tibet earthquake: Journal of Geophysical Research: Solid Earth, **112**, B06301, doi: 10.1029/2006JB004425.

Bilek, S. L., and T. Lay, 2018, Subduction zone megathrust earthquakes: Geosphere, **14**, no. 4, 1468–1500, doi: 10.1130/GES01608.1.

Blenkinsop, T. G., 2008, Relationships between faults, extension fractures and veins, and stress: Journal of Structural Geology, **30**, no. 5, 622–632, doi: 10.1016/j.jsg.2008.01.008.

Bonini, M., D. Sokoutis, G. Mulugeta, and E. Katrivanos, 2000, Modelling hanging wall accommodation above rigid thrust ramps: Journal of Structural Geology, **22**, no. 8, 1165–1179, doi: 10.1016/S0191-8141(00)00033-X.

Boston, B., G. F. Moore, Y. Nakamura, and S. Kodaira, 2017, Forearc slope deformation above the Japan Trench megathrust: Implications for subduction erosion: Earth and Planetary Science Letters, **462**, 26–34, doi: 10.1016/j.epsl.2017.01.005.

Brodsky, E. E., J. J. Gilchrist, A. Sagy, and C. Collettini, 2011, Faults smooth gradually as a function of slip: Earth and Planetary Science Letters, **302**, no. 1-2, 185–193, doi: 10.1016/j.epsl.2010.12.010.

Brodsky, E. E., and N. J. van der Elst, 2014, The uses of dynamic earthquake triggering: Annual Review of Earth and Planetary Sciences, **42**, 317–339, doi: 10.1146/annurev-earth-060313-054648.

Bürgmann, R., 2018, The geophysics, geology and mechanics of slow fault slip: Earth and Planetary Science Letters, **495**, 112–134, doi: 10.1016/j.epsl.2018.04.062.

Bürgmann, R., D. D. Pollard, and S. J. Martel, 1994, Slip distributions on faults: effects of stress gradients, inelastic deformation, heterogeneous host-rock stiffness, and fault interaction: Journal of Structural Geology, **16**, no. 12, 1675–1690, doi: 10.1016/0191-8141(94)90134-1.

Byrne, D. E., D. M. Davis, and L. R. Sykes, 1988, Loci and maximum size of thrust earthquakes and the mechanics of the shallow region of subduction zones: Tectonics, **7**, no. 4, 833–857, doi: 10.1029/TC007i004p00833.

Caine, J. S., J. P. Evans, and C. B. Forster, 1996, Fault zone architecture and permeability structure: Geology, **24**, no. 11, 1025–1028, doi: 10.1130/0091-7613(1996)024<1025:FZAAPS>2.3.CO;2.

Chi, W. C., and E. Hauksson, 2006, Fault-perpendicular aftershock clusters following the 2003 Mw = 5.0 Big Bear, California, earthquake: Geophysical Research Letters, **33**, L07301, doi: 10.1029/2005GL025033.

Cho, S. H., Y. Ogata, and K. Kaneko, 2003, Strain-rate dependency of the dynamic tensile strength of rock: International Journal of Rock Mechanics and Mining Sciences, **40**, no. 5, 763–777, doi: 10.1016/S1365-1609(03)00072-8.

Collettini, C., T. Tesei, M. M. Scuderi, B. M. Carpenter, and C. Viti, 2019, Beyond Byerlee friction, weak faults and implications for slip behavior: Earth and Planetary Science Letters, **519**, 245-263, doi: 10.1016/j.epsl.2019.05.011.

Dahlen, F. A., 1984, Noncohesive critical Coulomb wedges: An exact solution: Journal of Geophysical Research: Solid Earth, **89**, B12, 10125–10133, doi: 10.1029/JB089iB12p10125.

Dahlen, F. A., J. Suppe, and D. Davis, 1984, Mechanics of fold-and-thrust belts and accretionary wedges: Cohesive Coulomb theory: Journal of Geophysical Research: Solid Earth, **89**, B12, 10087–10101, doi: 10.1029/JB089iB12p10087.

Das, S., 1992, Reactivation of an oceanic fracture by the Macquarie Ridge earthquake of 1989: Nature, **357**, 150–153, doi: 10.1038/357150a0.

Das, S., 2019, Unusual large earthquakes on oceanic transform faults, *in* A. Bizzarri, S. Das, and A. Petri, eds., Mechanics of Earthquake Faulting: Proceedings of the International School of Physics "Enrico Fermi" **202**, 33–52, doi: 10.3254/978-1-61499-979-9-33.

Das, S., and C. Henry, 2003, Spatial relation between main earthquake slip and its aftershock distribution: Reviews of Geophysics, **41**, no. 3, doi: 10.1029/2002RG000119.

Davis, D., J. Suppe, F. A. Dahlen, 1983, Mechanics of fold-and-thrust belts and accretionary wedges: Journal of Geophysical Research: Solid Earth, **88**, B2, 1153–1172, doi: 10.1029/JB088iB02p01153.

Davis, G. H., A. P. Bump, P. E. García, and S. G. Ahlgren, 1999, Conjugate Riedel deformation band shear zones: Journal of Structural Geology, **22**, no. 2, 169–190, doi: 10.1016/S0191-8141(99)00140-6.

Di Toro, G., R. Han, T. Hirose, N. De Paola, S. Nielsen, K. Mizoguchi, F. Ferri, M. Cocco, and T. Shimamoto, 2011, Fault lubrication during earthquakes: Nature, **471**, 494–498, doi: 10.1038/nature09838.

Dmowska, R., and B. V. Kostrov, 1973, A shearing crack in a semi-space under plane strain conditions: Archives of Mechanics, **25**, 421–440.

Dominguez, S., J. Malavieille, and S. E. Lallemand, 2000, Deformation of accretionary wedges in response to seamount subduction: Insights from sandbox experiments: Tectonics, **19**, no. 1, 182–196, doi: 10.1029/1999TC900055.

Dunham, E. M., D. Belanger, L. Cong, and J. E. Kozdon, 2011, Earthquake ruptures with strongly rate-weakening friction and off-fault plasticity, Part 2: Nonplanar faults: Bulletin of the Seismological Society of America, **101**, no. 5, 2308–2322, doi: 10.1785/0120100076.

Faulkner, D. R., C. A. L. Jackson, R. J. Lunn, R. W. Schlische, Z. K. Shipton, C. A. J. Wibberley, and M. O. Withjack, 2010, A review of recent developments concerning the structure, mechanics and fluid flow properties of fault zones: Journal of Structural Geology, **32**, no. 11, 1557–1575, doi: 10.1016/j.jsg.2010.06.009.

Fineberg, J., and M. Marder, 1999, Instability in dynamic fracture: Physics Reports, **313**, no. 1-2, 1–108, doi: 10.1016/S0370-1573(98)00085-4.

Freund, L. B., 1998, Dynamic fracture mechanics: Cambridge University Press.

Fukuyama, E., 2015, Dynamic faulting on a conjugate fault system detected by near-fault tilt measurements: Earth, Planets and Space, **67**, 38, doi: 10.1186/s40623-015-0207-1.

Gabuchian, V., A. J. Rosakis, H. S. Bhat, R. Madariaga, and H. Kanamori, 2017, Experimental evidence that thrust earthquake ruptures might open faults: Nature, **545**, 336–339, doi: 10.1038/nature22045.

Geist, E. L., and R. Dmowska, 1999, Local tsunamis and distributed slip at the source: Pure and Applied Geophysics, **154**, no. 3-4, 485–512, doi: 10.1007/s000240050241.

Goebel, T. H., G. Kwiatek, T. W. Becker, E. E. Brodsky, and G. Dresen, 2017, What allows seismic events to grow big?: Insights from b-value and fault roughness analysis in laboratory stick-slip experiments: Geology, **45**, no. 9, 815–818, doi: 10.1130/G39147.1.

Green II, H. W., F. Shi, K. Bozhilov, G. Xia, and Z. Reches, 2015, Phase transformation and nanometric flow cause extreme weakening during fault slip: Nature Geoscience, **8**, 484–489, doi: 10.1038/ngeo2436.

Hananto, N. D., F. Leclerc, L. Li, M. Etchebes, H. Carton, P. Tapponnier, Y. Qin, P. Avianto, S. C. Singh, S. Wei, 2020, Tsunami earthquakes: Vertical pop-up expulsion at the forefront of subduction megathrust: Earth and Planetary Science Letters, **538**, 116197, doi: 10.1016/j.epsl.2020.116197.

Hasegawa, A., K. Yoshida, Y. Asano, T. Okada, T. Iinuma, and Y. Ito, 2012, Change in stress field after the 2011 great Tohoku-Oki earthquake: Earth and Planetary Science Letters, **355-356**, 231–243, doi: 10.1016/j.epsl.2012.08.042.

Hauksson, E., L. M. Jones, K. Hutton, and D. Eberhart-Phillips, 1993, The 1992 Landers earthquake sequence: Seismological observations: Journal of Geophysical Research: Solid Earth, **98**, B11, 19835–19858, doi: 10.1029/93JB02384.

Henry, C., S. Das, and J. H. Woodhouse, 2000, The great March 25, 1998, Antarctic Plate earthquake: Moment tensor and rupture history: Journal of Geophysical Research: Solid Earth, **105**, B7, 16097–16118, doi: 10.1029/2000JB900077.

Hill, R., 1950, The mathematical theory of plasticity: Clarendon Press, Oxford.

Hubbard, J., S. Barbot, E. M. Hill, and P. Tapponnier, 2015, Coseismic slip on shallow décollement megathrusts: Implications for seismic and tsunami hazard: Earth-Science Reviews, **141**, 45–55, doi: 10.1016/j.earscirev.2014.11.003.

Hudnut, K. W., L. Seeber, and J. Pacheco, 1989, Cross-fault triggering in the November 1987 Superstition Hills earthquake sequence, southern California: Geophysical Research Letters, **16**, no. 2, 199–202, doi: 10.1029/GL016i002p00199.

Hyndman, R. D., M. Yamano, and D. A. Oleskevich, 1997, The seismogenic zone of subduction thrust faults: Island Arc, **6**, 244–260, doi: 10.1111/j.1440-1738.1997.tb00175.x.

Ide, S., A. Baltay, and G. C. Beroza, 2011, Shallow dynamic overshoot and energetic deep rupture in the 2011 $M_w$ 9.0 Tohoku-Oki earthquake: Science, **332**, 1426–1429, doi: 10.1126/science.1207020.

Jamtveit, B., A. Petley-Ragan, S. Incel, K. G. Dunkel, C. Aupart, H. Austrheim, F. Corfu, L. Menegon, and F. Renard, 2019, The effects of earthquakes and fluids on the metamorphism of the lower continental crust: Journal of Geophysical Research: Solid Earth, **124**, 7725–7755, doi: 10.1029/2018JB016461.

Karakostas, V. G., E. E. Papadimitriou, G. F. Karakaisis, C. B. Papazachos, E. M. Scordilis, G. Vargemezis, and E. Aidona, 2003, The 2001 Skyros, Northern Aegean, Greece, earthquake sequence: off-fault aftershocks, tectonic implications, and seismicity triggering: Geophysical Research Letters, **30**, no. 1, 1012, doi: 10.1029/2002GL015814.

Ke, C. Y., G. C. McLaskey, and D. S. Kammer, 2018, Rupture termination in laboratory-generated earthquakes: Geophysical Research Letters, **45**, 12,784–12,792, doi: 10.1029/2018GL080492.

Keren, T. T., and J. D. Kirkpatrick, 2016, The damage is done: Low fault friction recorded in the damage zone of the shallow Japan Trench décollement: Journal of Geophysical Research: Solid Earth, **121**, 3804–3824, doi: 10.1002/2015JB012311.

Kim, Y. S., D. C. Peacock, and D. J. Sanderson, 2004, Fault damage zones: Journal of Structural Geology, **26**, no. 3, 503–517, doi: 10.1016/j.jsg.2003.08.002.

King, G., and J. Náběkek, 1985, Role of fault bends in the initiation and termination of earthquake rupture: Science, **228**, no. 4702, 984–987, doi: 10.1126/science.228.4702.984.

Kirkpatrick, J. D., and C. D. Rowe, 2013, Disappearing ink: How pseudotachylytes are lost from the rock record: Journal of Structural Geology, **52**, 183–198, doi: 10.1016/j.jsg.2013.03.003.

Kodaira, S., T. No, Y. Nakamura, T. Fujiwara, Y. Kaiho, S. Miura, N. Takahashi, Y. Kaneda, and A. Taira, 2012, Coseismic fault rupture at the trench axis during the 2011 Tohoku-oki earthquake: Nature Geoscience, **5**, 646–650, doi: 10.1038/ngeo1547.

Lay, T., 2018, Reactivation of oceanic fracture zones in large intraplate earthquakes? *in* J. C. Duarte, ed., Transform Plate Boundaries and Fracture Zones, New York: Elsevier, 89–104, doi: 10.1016/B978-0-12-812064-4.00004-9.

Li, H., J. Pan, A. Lin, Z. Sun, D. Liu, J. Zhang, C. Li, K. Liu, M. L. Chevalier, K. Yun, and Z. Gong, 2016, Coseismic surface ruptures associated with the 2014 $M_w$ 6.9 Yutian earthquake on the Altyn Tagh fault, Tibetan Plateau: Bulletin of the Seismological Society of America, **106**, no. 2, 595–608, doi: 10.1785/0120150136.

Liao, Z., H. Liu, B. M. Carpenter, K. J. Marfurt, and Z. Reches, 2019, Analysis of fault damage zones using three-dimensional seismic coherence in the Anadarko Basin, Oklahoma: The American Association of Petroleum Geologists Bulletin, **103**, no. 8, 1771–1785, doi: 10.1306/1219181413417207.

Ma, S., 2012, A self-consistent mechanism for slow dynamic deformation and tsunami generation for earthquakes in the shallow subduction zone: Geophysical Research Letters, **39**, L11310, doi: 10.1029/2012GL051854.

Ma, S., and D. J. Andrews, 2010, Inelastic off-fault response and three-dimensional dynamics of earthquake rupture on a strike-slip fault: Journal of Geophysical Research: Solid Earth, **115**, B04304, doi: 10.1029/2009JB006382.

Ma, S., and E. T. Hirakawa, 2013, Dynamic wedge failure reveals anomalous energy radiation of shallow subduction earthquakes: Earth and Planetary Science Letters, **375**, 113–122, doi: 10.1016/j.epsl.2013.05.016.

Ma, X., and A. Elbanna, 2019, Dynamic rupture propagation on fault planes with explicit representation of short branches: Earth and Planetary Science Letters, **523**, 115702, doi: 10.1016/j.epsl.2019.07.005.

Marone, C., 1998, Laboratory-derived friction laws and their application to seismic faulting: Annual Review of Earth and Planetary Sciences, **26**, 643–696, doi: 10.1146/annurev.earth.26.1.643.

McLaskey, G. C., B. D. Kilgore, and N. M. Beeler, 2015, Slip-pulse rupture behavior on a 2 m granite fault: Geophysical Research Letters, **42**, no. 17, 7039–7045, doi: 10.1002/2015GL065207.

Meng, L., J. P. Ampuero, J. Stock, Z. Duputel, Y. Luo, and V. C. Tsai, 2012, Earthquake in a maze: Compressional rupture branching during the 2012 $M_w$ 8.6 Sumatra earthquake: Science, **337**, no. 6095, 724–726, doi: 10.1126/science.1224030.

Ngo, D., Y. Huang, A. Rosakis, W. A. Griffith, and D. Pollard, 2012, Off-fault tensile cracks: A link between geological fault observations, lab experiments, and dynamic rupture models: Journal of Geophysical Research: Solid Earth, **117**, B01307, doi: 10.1029/2011JB008577.

Nicholson, C., L. Seeber, P. Williams, and L. R. Sykes, 1986, Seismic evidence for conjugate slip and block rotation within the San Andreas Fault System, southern California: Tectonics, **5**, no. 4, 629–648, doi: 10.1029/TC005i004p00629.

Niemeijer, A., G. Di Toro, W. A. Griffith, A. Bistacchi, S. A. Smith, and S. Nielsen, 2012, Inferring earthquake physics and chemistry using an integrated field and laboratory approach: Journal of Structural Geology, **39**, 2–36, doi: 10.1016/j.jsg.2012.02.018.

Noda, A., 2016, Forearc basins: Types, geometries, and relationships to subduction zone dynamics: The Geological Society of America Bulletin, **128**, no. 5-6, 879–895, doi: 10.1130/B31345.1.

Okubo, K., H. S. Bhat, E. Rougier, S. Marty, A. Schubnel, Z. Lei, E. E. Knight, and Y. Klinger, 2019, Dynamics, radiation, and overall energy budget of earthquake rupture with coseismic off-fault damage: Journal of Geophysical Research: Solid Earth, **124**, 11771–11801, doi: 10.1029/2019JB017304.

Perrin, C., I. Manighetti, J. P. Ampuero, F. Cappa, and Y. Gaudemer, 2016, Location of largest earthquake slip and fast rupture controlled by along-strike change in fault structural maturity due to fault growth: Journal of Geophysical Research: Solid Earth, **121**, 3666–3685, doi: 10.1002/2015JB012671.

Petit, J. P., and M. Barquins, 1988, Can natural faults propagate under mode II conditions?: Tectonics, **7**, no. 6, 1243–1256, doi: 10.1029/TC007i006p01243.

Petley-Ragan, A., Y. Ben-Zion, H. Austrheim, B. Ildefonse, F. Renard, and B. Jamtveit, 2019, Dynamic earthquake rupture in the lower crust: Science Advances, **5**, no. 7, eaaw0913, doi: 10.1126/sciadv.aaw0913.

Poliakov, A. N., R. Dmowska, and J. R. Rice, 2002, Dynamic shear rupture interactions with fault bends and off-axis secondary faulting: Journal of Geophysical Research: Solid Earth, **107**, B11, 2295, doi: 10.1029/2001JB000572.

Pollard, D. D., and P. Segall, 1987, Theoretical displacements and stresses near fractures in rock: With applications to faults, joints, veins, dikes, and solution surfaces, *in* B. K. Atkinson, eds., Fracture Mechanics of Rock: Academic Press, London, United Kingdom, 277–349.

Preuss, S., R. Herrendörfer, T. Gerya, J. P. Ampuero, and Y. van Dinther, 2019, Seismic and aseismic fault growth lead to different fault orientations: Journal of Geophysical Research: Solid Earth, **124**, 8867–8889, doi: 10.1029/2019JB017324.

Rice, J. R., 1980, The mechanics of earthquake rupture, *in* A. M. Dzieswonski, and E. Boschi, eds., Physics of Earth's Interior: Italian Physical Society and North Holland, Amsterdam, 555–649.

Robinson, D. P., C. Henry, S. Das, and J. H. Woodhouse, 2001, Simultaneous rupture along two conjugate planes of the Wharton Basin earthquake: Science, **292**, no. 5519, 1145–1148, doi: 10.1126/science.1059395.

Rosenau, M., and O. Oncken, 2009, Fore-arc deformation controls frequency-size distribution of megathrust earthquakes in subduction zones: Journal of Geophysical Research: Solid Earth, **114**, B10311, doi: 10.1029/2009JB006359.

Ross, Z. E., E. Hauksson, Y. Ben-Zion, 2017, Abundant off-fault seismicity and orthogonal structures in the San Jacinto fault zone: Science Advances, **3**, no. 3, e1601946 doi: 10.1126/sciadv.1601946.

Ross, Z. E., B. Idini, Z. Jia, O. L. Stephenson, M. Zhong, X. Wang, Z. Zhan, M. Simons, E. J. Fielding, S. H. Yun, and E. Hauksson, 2019, Hierarchical interlocked orthogonal faulting in the 2019 Ridgecrest earthquake sequence: Science, **366**, no. 6463, 346–351, doi: 10.1126/science.aaz0109.

Rousseau, C. E., and A. J. Rosakis, 2003, On the influence of fault bends on the growth of sub-Rayleigh and intersonic dynamic shear ruptures: Journal of Geophysical Research: Solid Earth, **108**, 2411, doi: 10.1029/2002JB002310.

Rowe, C. D., and W. A. Griffith, 2015, Do faults preserve a record of seismic slip: A second opinion: Journal of Structural Geology, **78**, 1–26, doi: 10.1016/j.jsg.2015.06.006.

Scholz, C. H., 1998, Earthquakes and friction laws: Nature, **391**, 37–42, doi: 10.1038/34097.

Scholz, C. H., 2019, The mechanics of earthquakes and faulting (3rd Edition): Cambridge University Press.

Segall, P., and D. D. Pollard, 1983, Nucleation and growth of strike slip faults in granite: Journal of Geophysical Research: Solid Earth, **88**, B1, 555–568, doi: 10.1029/JB088iB01p00555.

Sibson, R. H., 1985, A note on fault reactivation: Journal of Structural Geology, **7**, 751–754, doi: 10.1016/0191-8141(85)90150-6.

Spray, J. G., 1995, Pseudotachylyte controversy: Fact or friction?: Geology, **23**, 1119–1122, doi: 10.1130/0091-7613(1995)023<1119:PCFOF>2.3.CO;2.

Spray, J. G., 2010, Frictional melting processes in planetary materials: From hypervelocity impact to earthquakes: Annual Review of Earth and Planetary Sciences, **38**, 221–254, doi: 10.1146/annurev.earth.031208.100045.

Talwani, P., 2014, Intraplate earthquakes: Cambridge University Press.

Tchalenko, J. S., 1970, Similarities between shear zones of different magnitudes: The Geological Society of America Bulletin, **81**, no. 6, 1625–1640, doi: 10.1130/0016-7606(1970)81[1625:SBSZOD]2.0.CO;2.

Templeton, E. L., and J. R. Rice, 2008, Off-fault plasticity and earthquake rupture dynamics: 1. Dry materials or neglect of fluid pressure changes: Journal of Geophysical Research: Solid Earth, **113**, B09306, doi:10.1029/2007JB005529.

Thatcher, W., and D. P. Hill, 1991, Fault orientations in extensional and conjugate strike-slip environments and their implications: Geology, **19**, no. 11, 1116–1120, doi: 10.1130/0091-7613(1991)019<1116:FOIEAC>2.3.CO;2.

Tsuji, T., K. Kawamura, T. Kanamatsu, T. Kasaya, K. Fujikura, Y. Ito, T. Tsuru, and M. Kinoshita, 2013, Extension of continental crust by anelastic deformation during the 2011 Tohoku-oki earthquake: The role of extensional faulting in the generation of a great tsunami: Earth and Planetary Science Letters, **364**, 44–58, doi: 10.1016/j.epsl.2012.12.038.

Tullis, T. E., 2007, Friction of rock at earthquake slip rates, *in* H. Kanamori eds., Treatise on Geophysics, Vol. 4, Elsevier, Amsterdam, The Netherlands, 131–152.

von Huene, R., C. R. Ranero, and P. Vannucchi, 2004, Generic model of subduction erosion: Geology, **32**, no. 10, 913–916, doi: 10.1130/G20563.1.

Wang, K., 2010, Finding fault in fault zones: Science, **329**, no. 5988, 152–153, doi: 10.1126/science.1192223.

Wang, K., and Y. Hu, 2006, Accretionary prisms in subduction earthquake cycles: The theory of dynamic Coulomb wedge: Journal of Geophysical Research: Solid Earth, **111**, B06410, doi: 10.1029/2005JB004094.

Wang, K., Y. Hu, R. von Huene, and N. Kukowski, 2010, Interplate earthquakes as a driver of shallow subduction erosion: Geology, **38**, no. 5, 431–434, doi: 10.1130/G30597.1

Wibberley, C. A. J., G. Yielding, and G. Di Toro, 2008, Recent advances in the understanding of fault zone internal structure: a review, *in* C. A. J. Wibberley, W. Kurz, J. Imber, R. E. Holdsworth, and C. Collettini, eds., The Internal structure of fault zones: Implications for mechanical and fluid-flow properties, **299**, 5–33, doi: 10.1144/SP299.2.

Wilcox, R. E., T. P. Harding, and D. R. Seely, 1973, Basic wrench tectonics: The American Association of Petroleum Geologists Bulletin, **57**, no. 1, 74–96.

Xu, S., and Y. Ben-Zion, 2013, Numerical and theoretical analyses of in-plane dynamic rupture on a frictional interface and off-fault yielding patterns at different scales: Geophysical Journal International, **193**, no. 1, 304–320, doi: 10.1093/gji/ggs105.

Xu, S., E. Fukuyama, Y. Ben-Zion, and J. P. Ampuero, 2015, Dynamic rupture activation of backthrust fault branching: Tectonophysics, **644-645**, 161–183, doi: 10.1016/j.tecto.2015.01.011.

Xu, S., E. Fukuyama, H. Yue, and J. P. Ampuero, 2016, Simple crack models explain deformation induced by subduction zone megathrust earthquakes: Bulletin of the Seismological Society of America, **106**, no. 5, 2275–2289, doi: 10.1785/0120160079.

Xu, S., E. Fukuyama, F. Yamashita, K. Mizoguchi, S. Takizawa, and H. Kawakata, 2018, Strain rate effect on fault slip and rupture evolution: Insight from meter-scale rock friction experiments: Tectonophysics, **733**, 209–231, doi: 10.1016/j.tecto.2017.11.039.

Xu, S., E. Fukuyama, F. Yamashita, and S. Takizawa, 2019, Evolution of fault-interface Rayleigh wave speed over simulated earthquake cycles in the lab: Observations, interpretations, and implications: Earth and Planetary Science Letters, **524**, 115720, doi: 10.1016/j.epsl.2019.115720.

Yamashita, F., E. Fukuyama, S. Xu, K. Mizoguchi, H. Kawakata, and S. Takizawa, 2018, Rupture preparation process controlled by surface roughness on meter-scale laboratory fault: Tectonophysics, **733**, 193–208, doi: 10.1016/j.tecto.2018.01.034.

Yin, A., and T. K. Kelty, 2000, An elastic wedge model for the development of coeval normal and thrust faulting in the Mauna Loa-Kilauea rift system in Hawaii: Journal of Geophysical Research: Solid Earth, **105**, B11, 25909–25925, doi: 10.1029/2000JB900247.

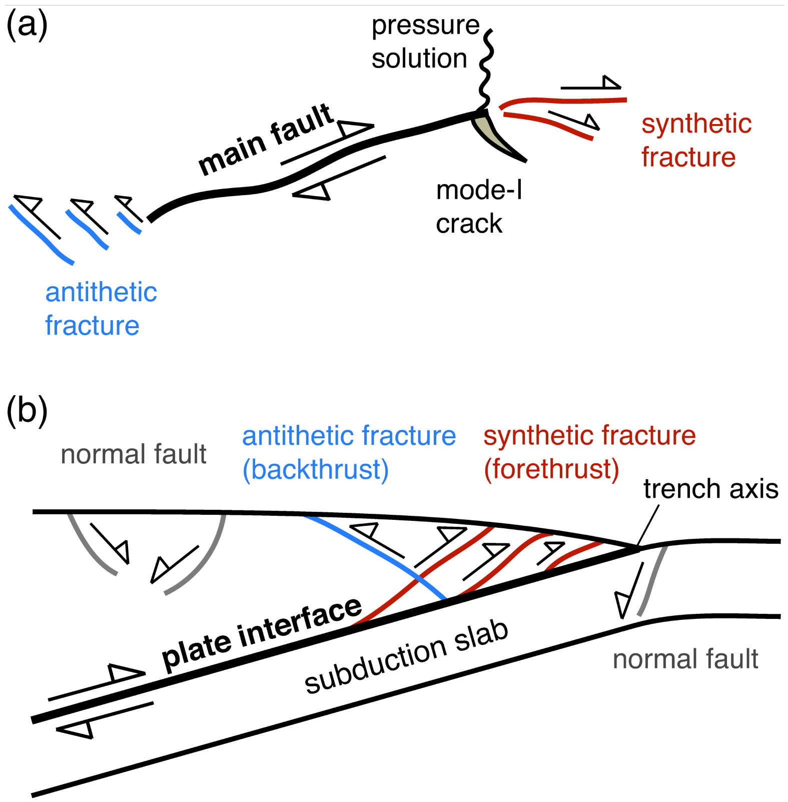


**Figure 1.** Schematic diagrams of fault zone structures for (a) a strike-slip fault system in map view and (b) a subduction-type thrust fault system in side view. Diagram in (a) is drawn based on Kim et al. (2004), and Pollard and Segall (1987); while diagram in (b) is drawn based on von Huene et al. (2004), Wang and Hu (2006), and Tsuji et al. (2013). The thickened curve in both (a) and (b) indicates the main fault.

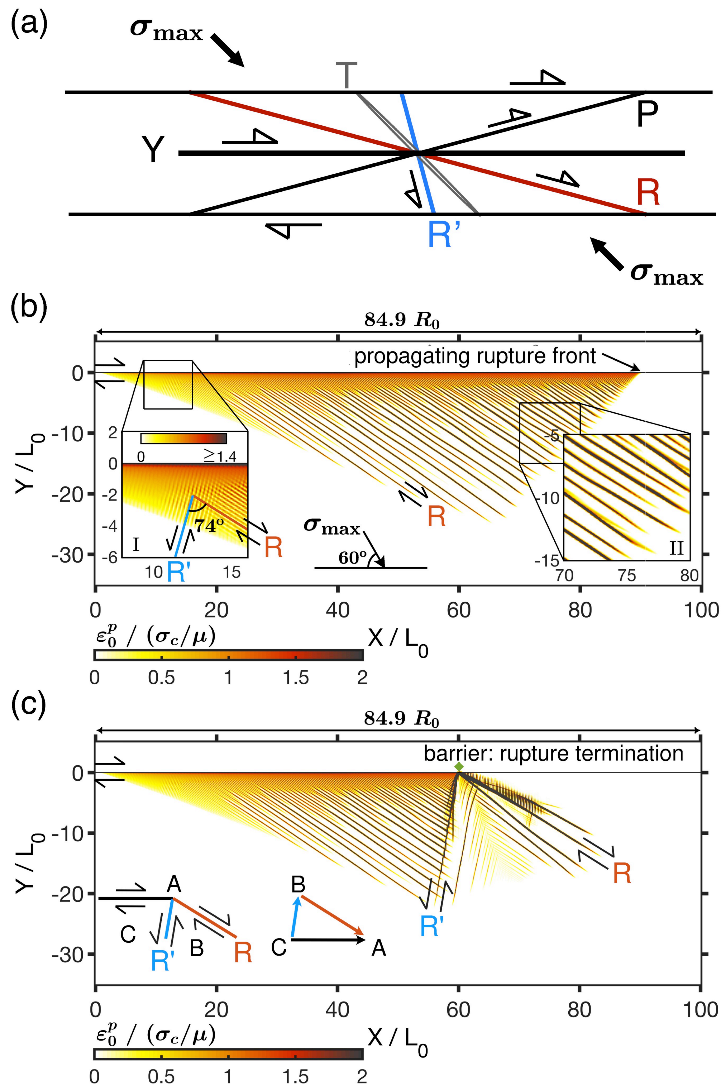


**Figure 2.** Riedel shear structures generated by static and dynamic loadings. (a) Schematic diagram of a classical Riedel shear system under quasi-static loadings, drawn based on Davis et al. (1999). $\sigma_{\max}$ denotes the background maximum principal stress. (b) Riedel shear structures (as plastic shear bands) generated by a propagating rupture along the fault. This figure is reproduced from Figure C1a in Xu and Ben-Zion (2013). (c) Riedel shear structures (as plastic shear bands) generated by a then propagating but now terminated rupture along the fault. This figure is reproduced from Figure 12a in Xu and Ben-Zion (2013). For results in (b) and (c), distance is normalized by $L_0$ (a reference length scale) or $R_0$ (the static process zone size). The amplitude of plastic strain $\varepsilon_0^p = \sqrt{2\varepsilon_{ij}^p \varepsilon_{ij}^p}$ is normalized by $\sigma_c/\mu$, where $\varepsilon_{ij}^p$ is the *ij*-th component of plastic strain, $\sigma_c$ is a reference stress, and $\mu$ is the shear modulus. See Xu and Ben-Zion (2013) for a detailed explanation of parameter settings. The inset diagram in (c) is drawn based on Figure 2 in King and Nábělek (1985), with capital letters A, B, and C denoting blocks separated by the main fault and shear fractures R and R'.

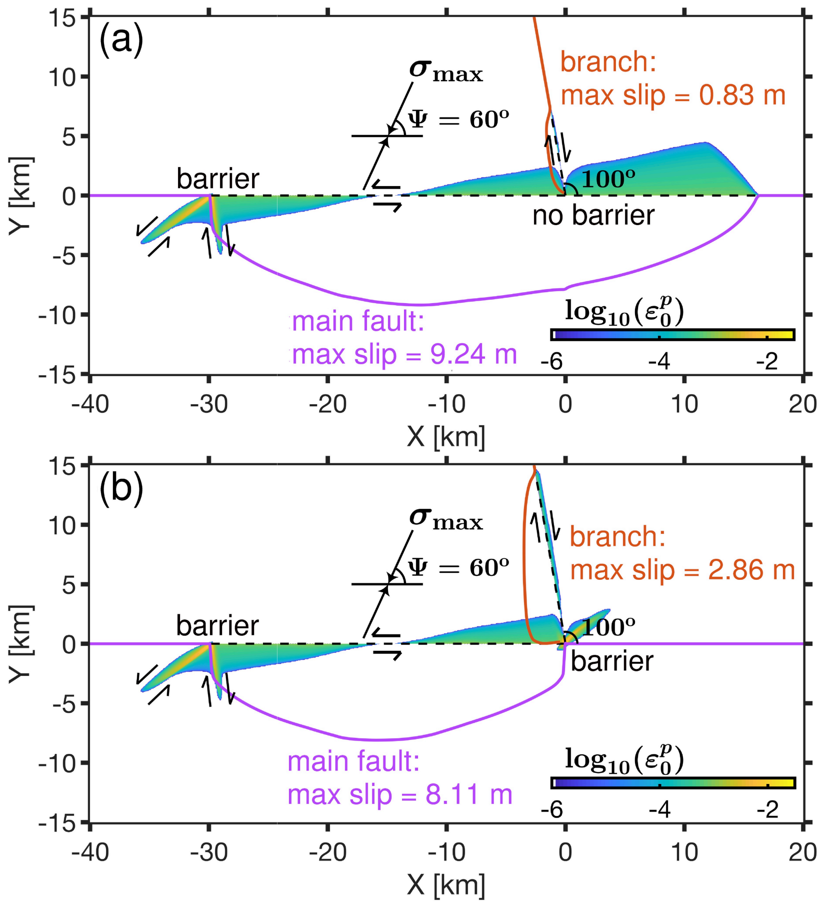


**Figure 3.** Rupture process and associated plastic strain distribution for a scenario (a) without a fault barrier and (b) with a fault barrier to the right direction of the main fault. For both (a) and (b), a fault barrier and a branch fault are inserted to the left and right directions of the main fault, respectively. Rupture is initiated at $\mathrm{X} = -15$ km along the main fault and then propagates bilaterally. The activation of the branch fault depends on the rupture dynamics along the main fault. Key parameter values are: $\sigma_{xx}^0 = -34.6$ MPa, $\sigma_{yy}^0 = -50$ MPa, $\sigma_{xy}^0 = -13.3$ MPa, $D_c^m = D_c^b = 0.5$ m, $f_s^m = f_s^b = 0.6$, $f_d^m = 0.1$, $f_d^b = 0.3$. Here $\sigma_{ij}^0$ represents the background stress (negative for compression or left-lateral shear along the *x*-axis). $D_c^k$, $f_s^k$, $f_d^k$ represent respectively the slip-weakening distance, the static friction coefficient, and the dynamic friction coefficient ($k = m$ for the main fault while $k = b$ for the branch fault). To model the barrier along the main fault, a spatial increase of $f_s^m$ from 0.6 to 5.0 is introduced over a 100 m interval, around $\mathrm{X} = -30$ km and $\mathrm{X} = 0$ km (optional). For the medium, mass density $\rho = 2700\ \mathrm{kg/m^3}$, P wave velocity $C_p = 6000$ m/s, and S wave velocity $C_s = 3464$ m/s. For plasticity, the internal friction angle $\phi = 30.9638°$, the cohesion $c = 1.4$ MPa, and the relaxation timescale $T_v = 0.05$ s.

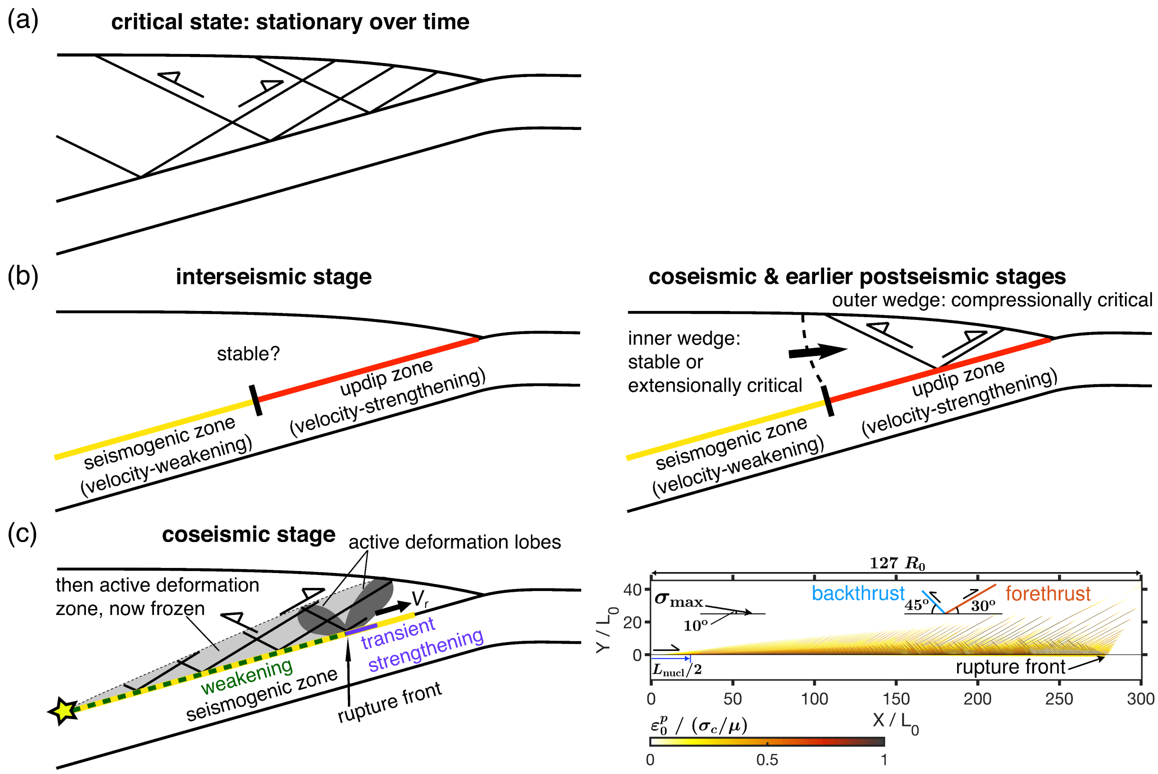


**Figure 4.** A comparison of three models for characterizing wedge deformation in subduction zones. (a) The wedge always stays at a critical state, according to the classical Coulomb wedge model. Depicted within the wedge are conjugate thrust faults that show an increased vertical extent towards the downdip direction. (b) During the interseismic stage (left), the wedge generally stays at a stable regime. During the coseismic and earlier postseismic stages (right), the inner wedge retains a stable state or enters an extensionally critical state, whereas the outer wedge is pushed into a compressionally critical state. This is the dynamic Coulomb wedge model developed by Wang and Hu (2006). (c) Schematic (left) and numerical (right) illustrations of the activation of a series of splay faults above a coseismic rupture zone. The generated splay faults show an increased vertical extent towards the updip direction, until they saturate the local depth range of the wedge. The numerical result (right panel) is redrawn based on Figure 7a in Xu and Ben-Zion (2013).

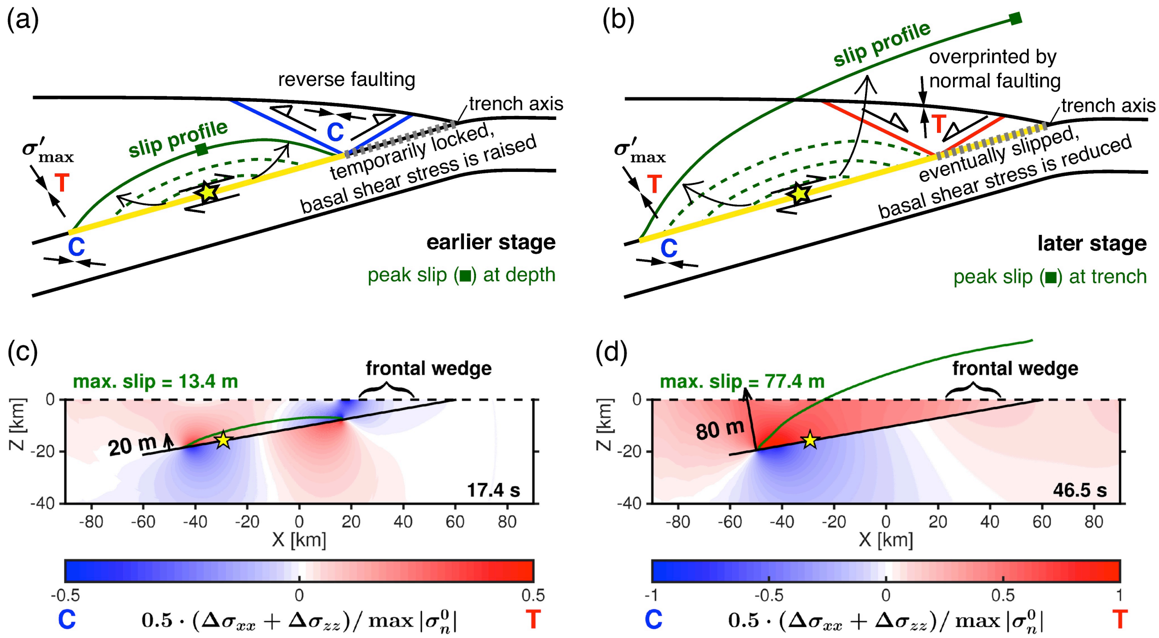


**Figure 5.** Slip evolution and deformation characteristics during a trench-breaking megathrust rupture. (a) and (b) schematically show the evolution of slip profiles (green curves) before and after the rupture reaches the trench, respectively. Star indicates the location of rupture hypocenter. Pair of arrows indicates the orientation of the in situ maximum principal stress $\sigma'_{\max}$, which can show a great variation in both space and time. (c) and (d) show the simulated results of mean stress change before and after the rupture reaches the trench, respectively. For all panels, capital letters C and T denote compressional and extensional stress changes, respectively. Panels (a)-(d) are redrawn based on Figure 8 in Xu et al. (2016). Parameter settings for producing the results in panels (c) and (d) can be found in Xu et al. (2016).